UTAH DEPARTMENT of ENVIRONMENTAL QUALITY

Quantitative Attribution of Wildfires on Summertime Ozone Concentrations along the Wasatch Front

Final Report

Prepared by:

Adam K. Kochanski
San Jose State University
Dept. of Meteorology and Climate Science
San Jose, CA 95192

Derek V. Mallia
University of Utah
Dept. of Atmospheric Sciences
Salt Lake City, UT 84112

Kerry E. Kelly
University of Utah
Dept. of Chemical Engineering
Salt Lake City, UT 84112

Jeremey Ranch, Utah, looking at the 2021 Parlays Canyon Fire

Submitted on July 1, 2022

Abstract:

It is suspected that increasing wildland fire activity is deteriorating air quality across the Western U.S. Wildland fires emit many pollutants such as fine particulates and chemical precursors for ozone (O_3) formation. The chemical formation of O_3 during smoke events is poorly understood as many factors control O_3 production such as the type and amount of fuel being burned, availability of nitrogen oxides and volatile organic compounds, as well as smoke shading effects. Air quality observations of O_3, particulate matter with a diameter of less than 2.5 microns ($PM_{2.5}$), and carbon monoxide (CO) were combined with model analyses generated by a coupled fire-atmosphere model (WRF-SFIRE-Chem) to explore how urban emissions interact with smoke to form O_3. Coupled fire-atmosphere models such as WRF-SFIRE-Chem can explicitly resolve many of the underlying physical and chemical processes that govern smoke transport. WRF-SFIRE-Chem simulations were able to reproduce regional smoke transport across the Western U.S for a smoke episode in August 2020. O_3 concentrations were elevated in areas under the influence of the smoke plume such as Boise, Idaho, and northern Utah. Simulations were also generated with and without aerosol radiative feedback to investigate the impacts of smoke shading on O_3 production. Simulations that included smoke shading resulted in O_3 concentrations that were lower relative to simulations that had aerosol radiative feedbacks turned off. Interestingly, turning on and off aerosol feedbacks not only changed the distribution of O_3 but also affected the transport of $PM_{2.5}$ and CO. These results suggest that smoke shading effects can alter regional meteorology and wind patterns within and around the smoke plume, which can ultimately impact smoke transport and smoke plume chemistry. An observational-based framework using low-cost sensors was also developed to investigate the August 2020 event. Preliminary results found that low-cost sensors, combined with two calibration models can accurately predict O_3 during wildfire smoke events. O_3 concentrations appeared to be highest near downtown Salt Lake City, and gradually decreased as the distance from the city increased.

Background and Significance:

Wildfires can enhance summertime ozone (O_3) and aerosol concentrations, which can degrade air quality and have adverse effects on human health. While air quality has improved across much of the U.S., the Western U.S. has seen more extreme air quality events, which can be partially attributed to an increase in wildfire activity (Westerling et al. 2006; McClure and Jaffe 2018). Fire activity and smoke emissions are expected to increase through the end of the 21st century (Spracklen et al. 2009), which will continue to deteriorate summer air quality (AQ) across the State of Utah. A dichotomy in AQ observations has been identified where summertime $PM_{2.5}$ in the Western U.S. was increasing in contrast to the eastern U.S, which has observed decreases in $PM_{2.5}$ (McClure and Jaffe 2018). Across Utah, air quality sites have observed an annual increase of 1.5 $\mu g\ m^{-3}$ for exceptional air quality events during the late summer (August-September), which coincides with the middle of the fire season (Wilmot et al. 2021). It is suspected that recent increases in fire activity are driving elevated $PM_{2.5}$ concentrations. While continued reductions of nitric oxides (NO_x) emissions have helped reduce O_3 across much of the U.S. (Jaffe et al. 2007), some areas across the Western U.S. are seeing an uptick in summertime O_3 by 2-8 ppb (Liu et al. 2017).

Disentangling the impacts of smoke on the urban landscape is challenging, as there are many processes that need to be accounted for. For smoke transport, these processes include: (1) the emission of smoke from combustion along the fire line, (2) fire-affected local meteorology, (3) the buoyant fire plume rise, (4) entrainment along the plume rises, (5) particle scavenging by

wet and dry deposition, (6) aerosol direct and indirect effects, and (7) the advection of smoke by larger-scale wind patterns (Figure 1). Many of the processes listed above interact and are dependent on each other. For example, the wildfire plume rise and the vertical dispersion of smoke are affected by the strength of the fire-emitted heat fluxes. Smoke can also directly interact with local and regional meteorology by shading areas underneath the wildfire smoke plume, which results in cooling and changes in wind patterns in and around the smoke plume (Kochanski et al. 2019).

There are many chemical compounds emitted from wildfires that can aid in the formation of O_3 (Yokelson et al. 2011). Wildfires smoke plumes are usually composed of elevated concentrations of O_3 precursors such as NO_x and especially volatile organic compounds (VOCs). As a result, smoke plumes can have O_3 enhancements that range from 0 to 90 ppb (Verma et al. 2009). O_3 production within wildfire smoke plumes can be sensitive to a variety of variables such as time of day, meteorology, altitude, the chemical composition of the plume, combustion efficiency, transport (residence time), and proximity to other emission sources. Smoke plume chemistry can also be impacted by smoke shading effects, which can reduce the amount of sunlight available for O_3 photochemistry. Previous work has suggested that surface $PM_{2.5}$ concentrations that exceed 50 μg m^{-3} are indicative of a smoke plume that is thick enough to reduce O_3 production (Buysse et al. 2019). Smoke plumes that intersect urban centers can also see further O_3 enhancements when the smoke plume interacts with NO_x-rich environments (Ninneman and Jaffe 2021).

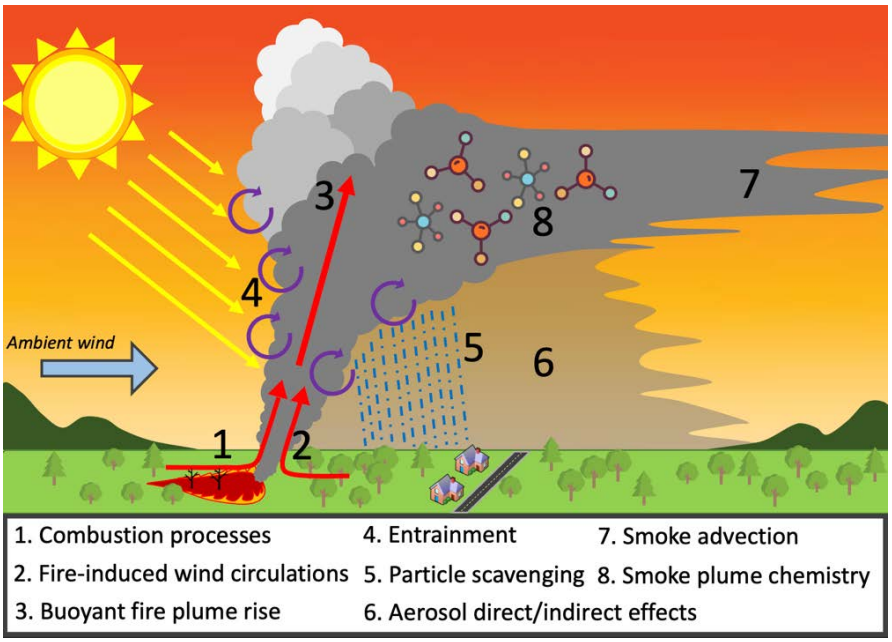

Figure 1. A schematic illustrating processes important in the context of smoke transport, dispersion, and chemistry.

The complexity of the underlying physical and chemical processes surrounding smoke transport and smoke impacts on urban quality motivates the research utilizing high-resolution atmospheric transport models and high-density air quality measurements. For this project, we utilized a state-of-the-art coupled-fire atmosphere model (WRF-SFIRE; Mandel et al. 2011) to determine how wildfire smoke enhances O_3 concentrations across urban centers. WRF-SFIRE can account for and dynamically link many fire and smoke-related processes identified in Figure 1. For example, fire growth within WRF-SFIRE is parameterized using a semi-empirical formula that relates local meteorology, fuel types, characteristics, and terrain to fire growth rates. The simulated fire growth within WRF-SFIRE is then used to compute smoke emissions and heat fluxes, which are injected into the atmosphere. Heat fluxes computed by WRF-SFIRE are added to the atmosphere, which allows the model to generate a buoyant smoke plume. The

explicit representation of the wildfire plume rise within WRF-SFIRE allows the model to loft smoke into the atmosphere (Figure 2) in response to the fire heat fluxes. Typically, WRF-SFIRE is run at a grid spacing equal to or less than 1.5-km, which allows the model to explicitly resolve the wildfire plume rise for larger fires (Kochanski et al. 2019; 2021).

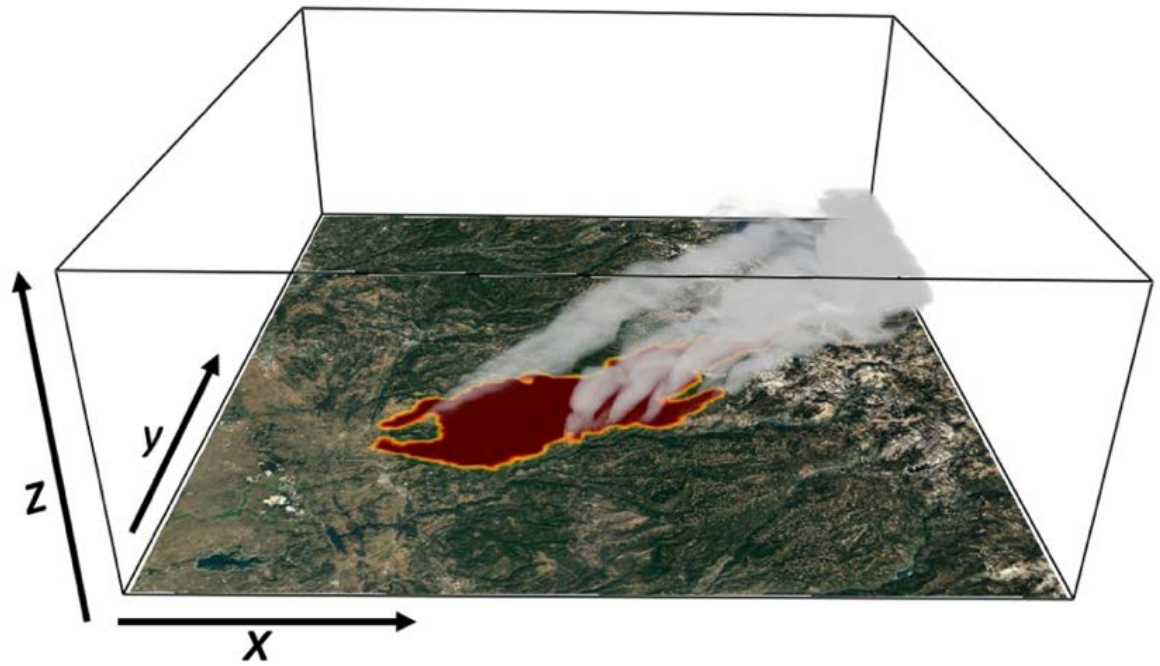

Figure 2. WRF-SFIRE forecast for the Caldor Fire in California during the 2021 wildfire season. The red area shows the modeled burned area while the transparent gray isosurfaces represents smoke ($PM_{2.5}$).

WRF-SFIRE has been coupled with WRF-CHEM (Grell et al. 2005) so that smoke produced from the wildfire can chemically interact with other chemical species found in the atmosphere (WRF-SFIRE-CHEM; Kochanski et al. 2016). For the remainder of this report, WRF-SFIRE-Chem will be abbreviated as WRFSFC. WRFSFC can also account for aerosol interactions such as radiative feedbacks, where aerosols can absorb/scatter/and reflect incoming solar radiation, as well as wet and dry deposition, which removes scavenges particulate matter from the atmosphere (Kochanski et al. 2019). Since WRFSFC can account for many of the processes outlined in Figure 1 and couples them under a unified framework, WRFSFC is an ideal tool for studying smoke impacts on air quality.

Given the spatial heterogeneity of wildfire smoke plumes, low-cost sensors are also being recognized as being powerful tools allowing for investigations of how the transport of smoke and how smoke interacts with urban emissions (Mallia et al. 2021). Low-cost sensor measurements have been previously used to estimate $PM_{2.5}$ concentrations within wildfire smoke plumes at high spatial resolution across urban landscapes. Recent advances in the AirU oxidizing gas sensor, combined with calibration models, now allow low-cost sensors to estimate O_3 concentrations. These measurements provide insights into the spatial heterogeneity of O_3 measurements within wildfire smoke plumes that intersect urban centers like Salt Lake City (SLC).

Objective:

For this project, we deployed a coupled fire-atmosphere model with chemistry (WRFSFC) to simulate the downwind transport and chemical evolution of wildfire smoke. We

also used WRFSFC to investigate how wildfire smoke interacts with urban emissions. This high-resolution modeling framework simulated local and regional chemical transport processes, and complex fire-atmosphere interactions. This project also sought to use the oxidizing gas sensor located within low-cost sensors to assess spatial variability in O_3. Since low-cost sensors are cheaper relative to traditional O_3 monitoring instruments, many more of these sensors can be deployed across an urban center. Thus, low-cost sensors could be used to study localized O_3 gradients across the urban landscape. Through an analysis of observational and model data, this project specifically addressed the following scientific questions:

Scientific Questions:

1. What are the impacts of wildfires on ozone concentrations along the Wasatch Front relative to the contributions from anthropogenic sources?
2. How does smoke shading from smoke plumes impact photochemistry?
3. What is the spatial variability and sensitivity of smoke-enhanced ozone to different urban sources of ozone precursors?

We specifically addressed the 6th item in the Utah Division of Air Quality's (UDAQ) Goal and Priorities section, which encourages research on "*source contributions to summertime ozone*". Through this project, we identified the role that wildfire plays in enhancing summertime O_3 levels relative to other sources of pollutants, while also elucidating the complex chemical interactions between wildfire smoke and aerosol radiative feedbacks. In addition, this project also targeted the 1st and 3rd items in UDAQ's Goal and Priorities section, which seeks projects that can improve air quality models and elucidate air exchange processes that involve pollutants. To the best of our knowledge, *this project represents the first attempt to use a coupled fire-atmosphere model for air quality and photochemical modeling applications that includes all sources of atmospheric pollutants,* e.g., wildfires, anthropogenic sources, and biogenic emissions.

Methods:

The methodology section is broken up into two separate sections. The first section reviews the methodology behind how O_3 measurements were collected by the AirU low-cost sensors. The second section reviews the WRFSFC model configuration and setup. For this project, we selected a regional smoke event that impacted northern Utah from August 21st to 22th 2020. During this time, $PM_{2.5}$ ranged from 10-60 $\mu g\ m^{-3}$, while O_3 approached 100 ppb across northern parts of Utah. The source of the elevated $PM_{2.5}$ concentrations and the chemical

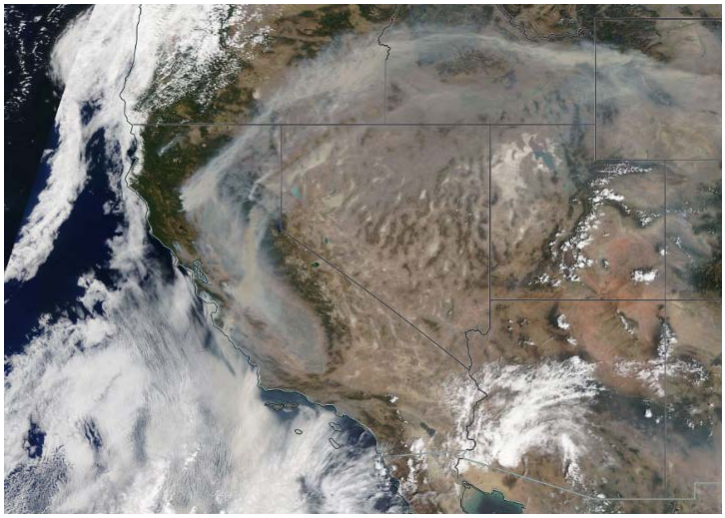

Figure 3. MODIS visible satellite image depicting a regional smoke event on August 21, 2020.

precursors that would have aided in the formation of O_3 likely originated from fire activity located in central and northern California (Figure 3).

AirU Ozone Sensor

The AirU sensor network had 68 sensors operational in the Salt Lake Valley (SLV) during a smoke event spanning from August 20-22, 2020. O_3 concentrations were estimated using two calibration models for 68 AirU sensors across the SLV. The metal oxide sensor on the AirU sensor is an SGX Sensortech MiCS-4514 compact MOS sensor that is equipped with two independent sensing elements, one for reducing species measurements (RED sensor) and one for oxidizing species measurements (OX sensor). Since O_3 is an oxidizing agent, it can be detected via the AirU OX sensor. In August 2020, 82 AirU sensors were operating across Salt Lake Valley. After the initial processing of AirU sensor measurements, 14 AirU sensors were dropped from the analysis. Three of the 14 sensors were dropped due to oxidizing measurements that ranged less than 100 mV compared to an average range of 600 mV. Values within this range indicate the possibility of a dirty sensor or a faulty resistive heater. 11 other sensors were discarded from this analysis as they reported many null measurements throughout the collection period. Null measurements indicate that the sensors either had a faulty metal oxide sensor, experienced a loss of power, or had some other type of problem. Measurements from the remaining 68 AirU sensors were resampled to hourly averages. Measurements collected by the AirU sensors were then aligned with hourly averaged DAQ O_3 and solar radiation measurements (Sayahi et al. 2020).

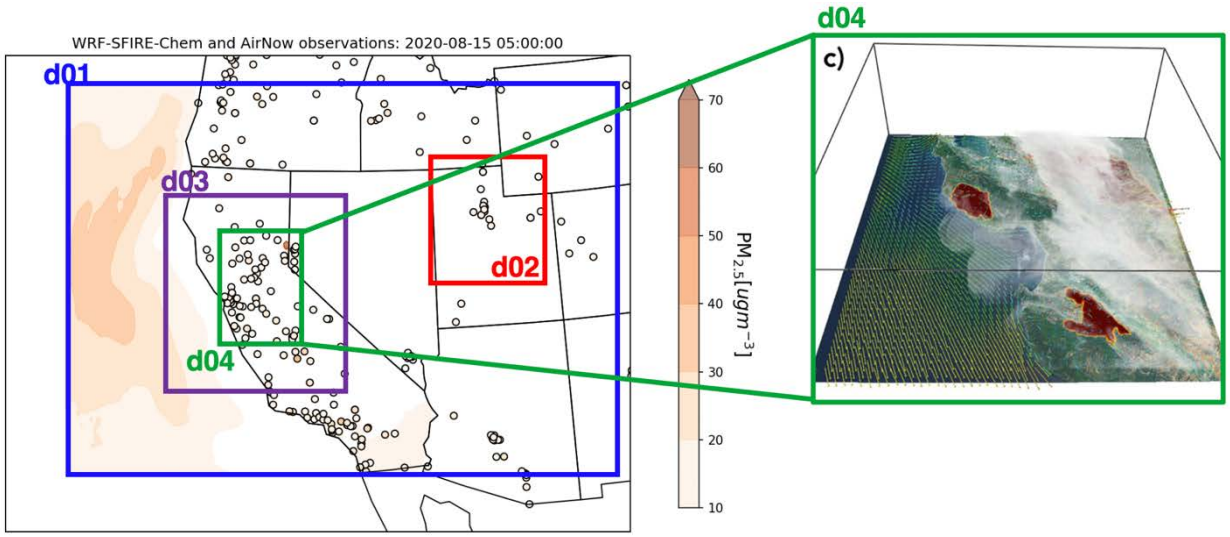

Figure 4. WRFSFC domain configuration for the August 21-25 smoke event simulation. Domain 1 (d01) had a grid spacing of 12-km, while domain 2 and 3 (d02 & d03) used a grid spacing of 4-km. Domain 4, which was centered over the fires producing smoke in central/northern California, had a grid spacing of 1.333-km to allow WRFSFC to explicitly resolve the wildfire plume rise. Colored circles represent AirNow air quality sites used to evaluate our WRFSFC model simulations.

A z-score normalization process was also used to address the inherent intra-sensor variability seen in metal oxide low-cost sensors (Okorn and Hannigan 2021). Applying the z-score normalization to each input variable resulted in each variable having the same order of magnitude. Furthermore, machine learning algorithms are more effective at solving models when input variables are of similar magnitude (Guido and Muller 2016). The AirU temperature, AirU oxidizing species, and DAQ solar radiation variables were individually z-scored by subtracting the mean of the data collection period and then dividing this by the standard deviation for the

same collection period. The z-scored variable distribution will have a mean of zero and a standard deviation of one. The z-scored values were used to develop and train a calibration model. z-Score normalization was not applied to the DAQ-measured O_3 concentrations since these O_3 measurements were used to evaluate our calibration models.

WRFSFC model setup:

As described in the **Motivation and Objection Sections**, this project deployed WRFSFC to quantify the impacts of smoke on air quality across Utah. WRFSFC is a coupled fire-atmosphere model that links fire emissions to WRF-Chem's chemical mechanisms. This allows WRFSFC to simulate complex atmospheric chemistry such as O_3 formation, along with aerosol physics and aerosol interactions with solar radiation. For this project, we ran WRFSFC for the August 20-22 2020 smoke event, which impacted a large portion of the Western U.S. To allow sufficient time for our chemical initial conditions to spin up, the WRFSFC simulation period was extended to cover August 14-26. Our WRFSFC model was configured such that most of the Western U.S. was covered by a coarse 12-km model grid, which will be referred to as domain 1 (Figure 4). In addition, two telescopic domains were embedded within our WRFSFC simulation, where domains 3 and 4 had 4- and 1.333-km grid spacing, respectively, and were centered over the source of the wildfire smoke shown in Figure 3. It's worth noting that the domain centered over the fires needed to have a high enough resolution properly simulate the vertical transport of smoke by the wildfire plume rise. Work by Kochanski et al. (2019) suggested that a 1.333-km can accurately simulate wildfire plume rises for larger wildfires. Another higher resolution domain with 4-km grid spacing was centered over northern Utah (Figure 4). All WRFSFC domains were configured with two-way nesting, meaning that smoke can be exchanged between each of the model domains. For our WRFSFC simulations, we utilized the MOZART chemical mechanism (Emmons et al. 2010) coupled with the GOCART aerosol model.

To run WRFSFC, many inputs are needed to generate simulations of wildfire smoke. Inputs for our WRFSFC simulations included the following:

a) *High-resolution fuel, vegetation, and topography data for fires we are simulating*
b) *Fire detecting data for initializing and prescribing fire growth*
c) *Meteorological boundary/initial conditions*
d) *Chemical boundary/initial conditions*
e) *Anthropogenic and biogenic emissions*

High-resolution fuel, vegetation, and topographic data from LANDFIRE (https://landfire.gov) with 30-m grid spacing were used to initialize fire mesh within the innermost WRFSFC domain (domain 4, see Figure 4). This is the domain responsible for running the WRFSFC's fire spread model, which is then used to compute the fuel consumption. The amount of fuel that is consumed by the fire is dependent on the fuel classification as determined by the LANDFIRE fuel data. The fuel classification is also used to determine the emission factors of smoke across many different chemical species.

Traditionally, WRFSFC forecasts fire growth using the Rothermel fire spread model. For this project, we prescribed fire growth using a new satellite-informed data assimilation product that utilizes a support-vector machine learning algorithm (SVM). Using SVM, infrared fire detections from the Visible Infrared Imaging Radiometer Suite are used to construct a two-dimensional matrix that can estimate the fire arrival time for any given grid cell (Farguell et al. 2021). This algorithm constraints fire growth within WRFSFC and eliminates some of the fire growth errors typically observed when driving a fire model with local meteorology. On average,

SVM has a good agreement when evaluated with an independent fire perimeter data set (Farguell et al. 2021) and provides continuous fire progression data that can be used to constrain the fire model. The SVM technique has a relatively high probability of detection (0.86), and a low false alarm ratio (0.21). In addition to estimating fire growth for any given fire, SVM should also better estimate the fire emissions generated by WRFSFC since this technique constrains the fire area and thus, the amount of fuel that is burned by the model. This UDAQ project represents one of the first attempts to use SVM for fire-related air quality modeling applications. Meteorological initial and boundary conditions for our WRFSFC simulations were obtained from the Climate Forecast System Reanalysis (CFSR; Saha et al. 2014). Output from CAM-chem in CESMv2.0 provided our WRFSFC simulations with large-scale chemical boundary conditions (Buchholz et al. 2019). Since our WRFSFC model simulation used the MOZART chemical mechanism, we speciated output from CAM-chem so that it would be compatible with WRFSFC. Lateral boundary and initial conditions were processed using NCAR's mozbc code.

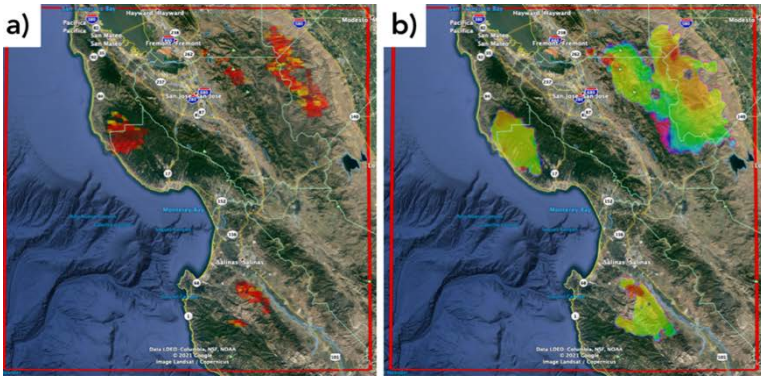

Figure 5. (a) Satellite estimated fire detections and the (b) SVM informed fire arrival time for fires located across the San Francisco Bay region on August 21 2020.

Anthropogenic emissions were obtained from the Environmental Protection Agency (EPA)'s National Emissions Inventory (NEI 2017) and regridded to conform with our WRFSFC model domain. NEI regridding and processing were carried out using NCAR's EPA_ANTHRO_EMIS tool. Like the CAM-chem processing, emissions from the 2017 NEI were speciated to be compatible with WRFSFC's MOZART chemical mechanism. The timestamps for the 2017 NEI emissions also had to be shifted so that the days of the week for 2017 were aligned with the days of the week in 2020. NCAR's EPA_ANTHRO_EMIS emission processing tool also had to be modified as there was a bug preventing emissions from being processed properly on grids that had a grid spacing of less than 4 km. Biogenic fluxes for chemical species like isoprene were obtained from MEGAN, which estimates the emission of gases and

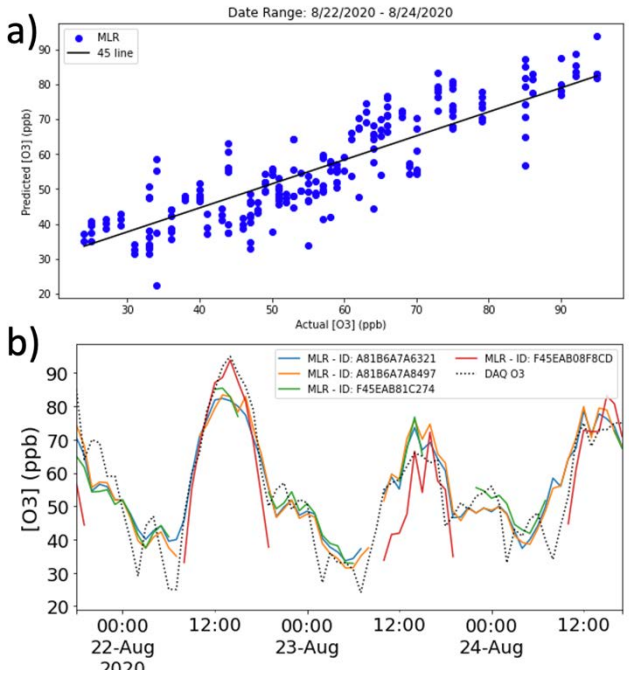

Figure 6. (a) A scatter showing the MLR model of the predicted O^3 concentrations from the four co-located AirU sensors for the training and test datasets vs. the reference DAQ O_3 measurement (R^2 = 0.72). (b) MLR model O^3 predictions from the four co-located AirU sensors shown against the DAQ O^3 measurement. The graph includes the DAQ O_3 measurement (black dotted line).

aerosols from terrestrial ecosystems (https://bai.ess.uci.edu/megan).

Once the WRFSFC simulations were configured, model simulations were generated for August 14-26th 2020. The first simulation, *which will be referred to as the baseline simulation*, included all sources of potential atmospheric pollutants (anthropogenic sources, background, biogenic, and wildfires) with aerosol radiative feedbacks turned on. Additional WRFSFC simulations were also carried out that turned off aerosol radiative feedbacks, turned off fire emissions, and turned off anthropogenic emissions. We compared each of these sensitivity simulations with each other to quantify the respective roles of wildfires, anthropogenic sources, and smoke shading effects in elevating or suppressing O_3 production during regional smoke events across Utah and surrounding areas. These results are reviewed in the following section.

Table 1. Performance metrics for the MLR (top table) and ANN model (bottom table) with z-score normalization compared to performance metrics for the model results with no z-score normalization.

Performance Metric	MLR model with z-score	MLR model without z-score
MSE (ppb^2)	72.8	100
RMSE (ppb)	8.53	10.0
Bias (%)	1.77	1.59
Precision (%)	21.32	22.9

Performance Metric	ANN model with z-score	ANN model without z-score
MSE (ppb^2)	63.2	205
RMSE (ppb)	7.95	14.3
Bias (%)	1.61	-14.7
Precision (%)	22.3	19.9

Results:

AirU Ozone Sensor Results

Two general calibration models were used to calibrate O_3 measurements for the AirU sensors. One method used a multiple linear regression (MLR) model while the second method used an artificial neural network (ANN) model. This model was calibrated based on O_3 measurements during the August 2020 wildfire smoke event and used inputs from four air quality sensors from the University of Utah's network of low-cost air quality sensors (AirU) co-located with a Utah Division of Air Quality (DAQ) reference monitor.

The equation below shows the final MLR model used to calibrate the AirU sensors to measure O_3:

$$O_{3,pred} = 56.09 + 12.48 * T_{z,AirU} - 7.16 * OX_{z,AirU} + 7.00 * SR_{z,DAQ}$$

where $O_{3,pred}$ is the predicted hourly O_3 concentration in ppb, $T_{z,AirU}$ is the hourly averaged z-scored AirU temperature measurement in degrees Celsius, $OX_{z,AirU}$ is the hourly averaged z-scored AirU OX signal measurement in millivolts, and $SR_{z,DAQ}$ is the hourly averaged z-scored DAQ station solar radiation measurement in Langley's per minute. The AirU OX signal coefficient is negative in the final version of the MLR model, because the AirU OX signal variable is counteracting the overshoot obtained from the AirU temperature variable. The linear regression with the AirU OX signal as the only variable has a positive coefficient for the AirU OX signal. Figure 6a shows a scatter plot for the MLR model and indicates a good correlation with the UDAQ O_3 concentration measurements. Figure 6b shows a time series of MLR predicted and UDAQ observed O_3. Overall, the MLR model captures the general shape and

magnitude of the UDAQ measured O_3 concentration. The MLR model performed well on the test dataset with a mean R^2 value and mean Root Mean Square Error (RMSE) value across the 5-folds of the cross-validation of 0.72 (+/- 0.13) and 8.7 ppb (+/ 0.8 ppb) respectively. Table 1 summarizes the MLR predictions from August 21-24, 2020. Additionally, the MLR model was recomputed without applying the z-score normalization process to analyze the impact that z-score normalization had on the O_3 concentration model predictions. Table 1 also shows the performance metrics computed for August 21-24, 2020 for both the MLR model with z-score normalization and with no z-score normalization. Overall, the MLR model with z-score normalization performed better than the MLR model with no z-score normalization. Figure 7a shows a colormap of the MLR predicted O_3 concentration for 2 pm, August 22, 2020, overlayed on a Salt Lake County Street map. Here, O_3 concentrations were the highest near downtown Salt Lake City while O_3 concentrations were lowest near the edges of the valley and further south.

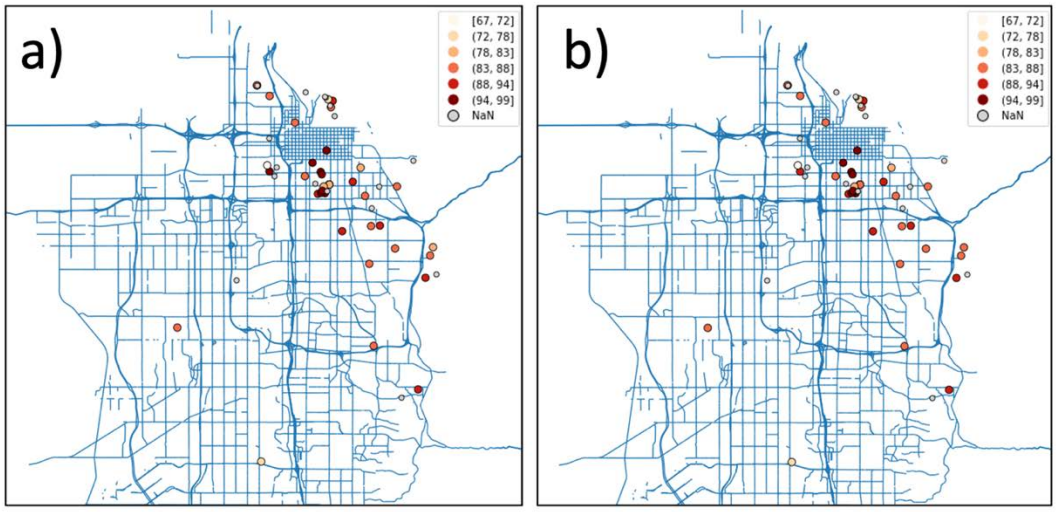

Figure 7. Geo-spatial plot of (a) MLR (b) and ANN predicted O_3 concentration for all 68 AirU sensors at 1400 LST on August 22, 2020.

The second calibration model we used to calibrate the AirU sensors utilized an ANN model. For the ANN model, we used the Mean Squared Error (MSE) and the Mean Absolute Error (MAE) for the selected loss and accuracy metrics, respectively. For our ANN model, we used the Adaptive Moment Estimation as our optimizer algorithm to train our neural network. An Epoch of 50 was chosen as our number of iterations while we used a batch size of 32. Our dropout rate for the ANN model was 20%. Finally, we used 25 neural nodes and 1 hidden layer. Figure 8 shows a scatter plot for the results from our ANN model and O_3 concentrations from select UDAQ measurement sites. Overall, this scatter plot showed relatively good agreement between UDAQ and ANN-predicted O_3 concentrations.

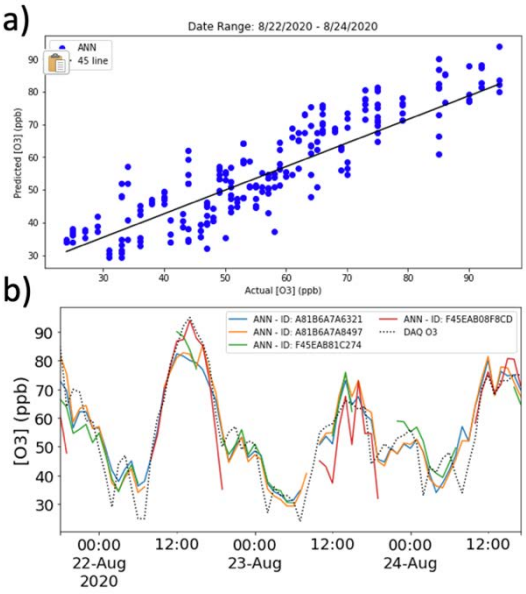

Figure 8. Same as Figure 6, but results from the ANN model. The correlation coefficient between the ANN model predicted and UDAQ O_3 concentrations was R^2 =0

Figure 7 shows the results of the ANN model and the Hawthorne DAQ station O_3 measurements. Like the MLR method, the ANN model also captures the general shape and magnitudes of the UDAQ reference O_3 measurements. The ANN model performed well on the test set and had a similar performance when compared with the MLR model. The ANN model had a mean R^2 and mean RMSE value across the 5-folds of the cross-validation of 0.73 (+/- 0.09) and 8.6 ppb (+/- 0.9 ppb), respectively. Table 1 shows the ANN model performance for August 21-24, 2020. Additionally, the ANN model was recomputed without applying the z-score normalization process to analyze the impact that z-score normalization had on the O_3 concentration model predictions. Table 1 lists the performance metrics for both the ANN model with and without z-score normalization. Overall, the ANN model using z-score normalization performed better than the ANN model with no z-score normalization. Figure 7a shows a colormap of the MLR predicted O_3 concentration for 2 pm, August 22, 2020, overlayed on a Salt Lake County Street map. Like the MLR model, O_3 concentrations were the highest near downtown SLC while O_3 concentrations were lowest near the edges of the valley and further south. This result is interesting in that previous work has shown that O_3 concentrations tend to titrate towards the middle of the valley due to heavier traffic emissions, which can create a localized NOx-limited environment (Mitchell et al. 2018). Since wildfire smoke is heavy in VOCs, it's plausible that the center of the valley is not NO_x limited during major smoke episodes.

To determine the fidelity of the low-cost sensor, the predicted O_3 concentrations from the AirU sensors were evaluated with an independent data set. The independent data set that we used here was from the TRAX mobile measurements (Mitchell et al. 2018). Comparison with TRAX train measurements provided an initial estimate of the calibration model performance. From this analysis, we sought to quantify relationships in O_3 between the AirU calibrated sensor and the TRAX train. It is important to note that this comparison is limited since the TRAX train measurements are instantaneous while the calibration model concentrations were averaged by the hour. Furthermore, the AirU sensors are not co-located with the TRAX train path of travel. Figures 9 show the time series and scatter plot for the MLR model (Figure 9a & b) and ANN model calibrated O_3 concentrations (Figure 9b & c) for a single AirU sensor. As seen in Figure 9, the MLR and ANN models for this AirU sensor captured the general shape and trend of O_3 concentrations measured by the instrument on the TRAX. The extent of correlation between the AirU ozone prediction and the TRAX train measurement was largely dependent on the sensor's distance from the TRAX train. The MLR and ANN model ozone hourly predictions were reasonably correlated with the TRAX train measurements with an average R^2 of 0.54 +/- 0.22 and 0.50 +/- 0.24, respectively. Given the limitations of this analysis described above, we

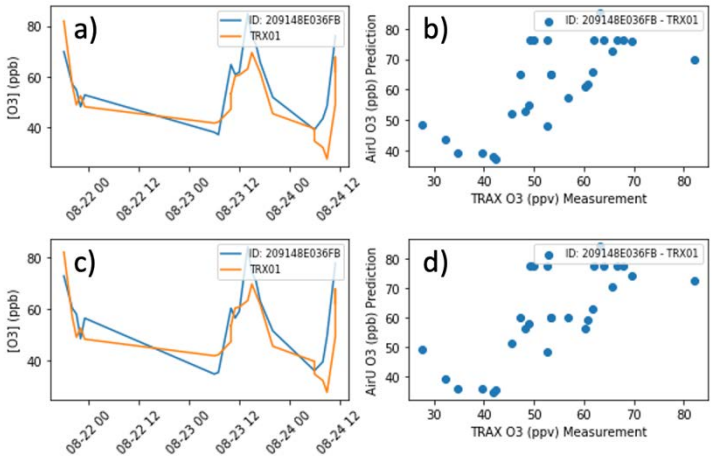

Figure 9. MLR (a & b) and ANN model (b & d) hourly averaged O_3 predictions results for one AirU sensor (ID: 209148E036FB) compared to the instantaneous O_3 measurements (30 second intervals) taken by TRAX train 01 when the train was located at a minimum distance from the AirU sensor. The minimum distance path of travel for TRAX train 01 is located 1.05 km from AirU sensor.

believe that the comparison to TRAX measurements does support the notion that the AirU sensors can reliably measure O_3 when calibrated using an MLR method or ANN model.

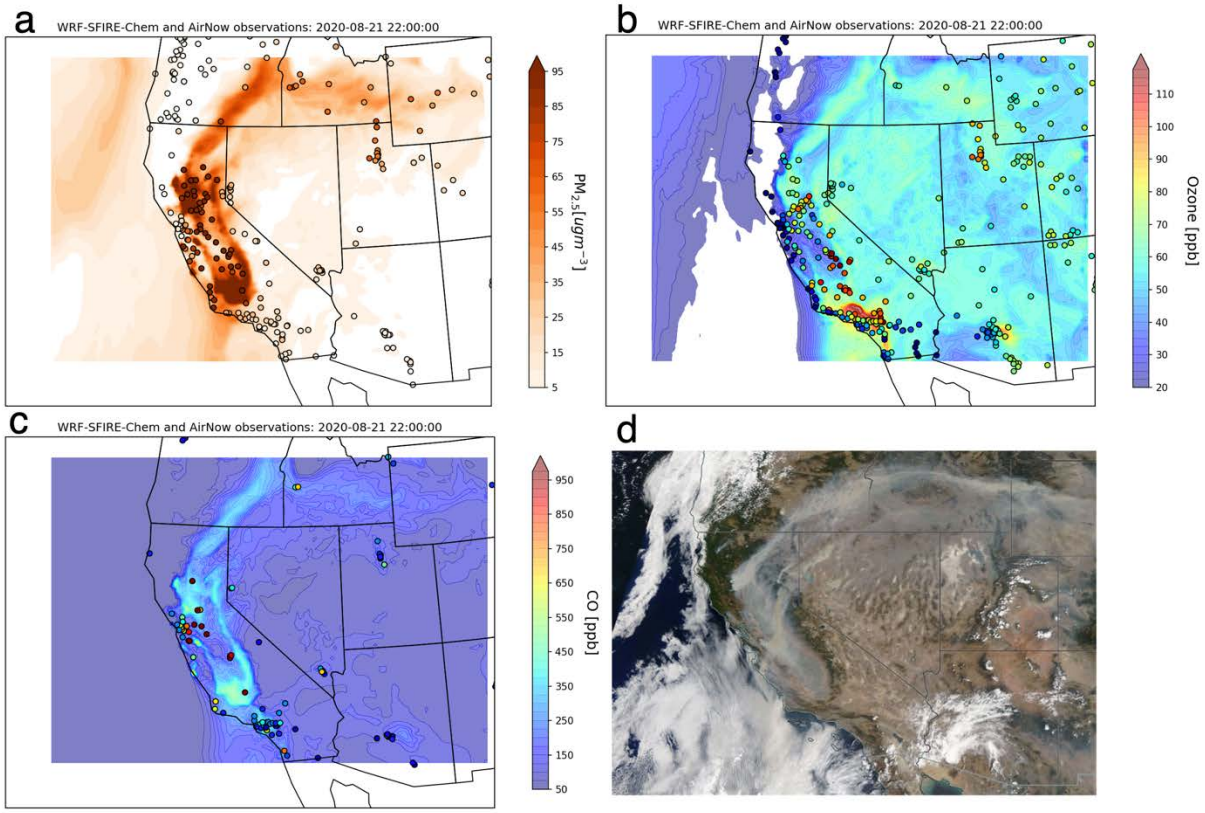

Figure 10. WRFSFC baseline simulations for (a) $PM_{2.5}$, (b) O_3, and (c) CO and a MODIS visible satellite image all for August 21, 2020. Colored circles represent observed concentrations for each respective pollutant ($PM_{2.5}$, O_3, and CO).

WRFSFC Simulation Results

As described in the **Objectives Section**, a series of WRFSFC simulations were carried out to quantify the role of wildfire smoke in O_3 production relative to other sources of atmospheric pollutants, e.g., anthropogenic emissions. We also sought to determine how smoke shading impacts O_3 within wildfire smoke plumes by comparing the baseline WRFSFC simulation with a simulation that turned off aerosol radiative feedbacks.

To reiterate from **Methodology Section**, the baseline WRFSFC simulation included all sources of atmospheric pollutants, e.g., wildfires, anthropogenic, and biogenic emissions. WRFSFC modeled concentrations of $PM_{2.5}$, CO, and O_3 were evaluated using measurements downloaded from the AirNow database (Figures 10 & 11). This analysis provided a regional assessment of how WRFSFC simulated smoke transport and chemistry. Regionally, fire activity was primarily confined to central and northern California during the middle of August, and was emitting a copious amount of smoke as seen in Figures 10 and 11. Between August 19-25th, a strong ridge was centered over the Intermountain West, which caused smoke to be transported from California towards SE Oregon and southern Idaho. Smoke continued to be advected to the east over Wyoming. According to air quality measurements across northern Utah, some of the smoke was advected southward along the Wasatch Front. Multiple sites across northern Utah measured $PM_{2.5}$ concentrations that exceeded 40 µg m^{-3} (Figure 10a). By August 22nd, the

regional smoke plume started to become diffuse due to decreased fire activity on August 21st (Figure 11a & d). Both observed and model-predicted $PM_{2.5}$ concentrations indicated a general lowering of $PM_{2.5}$ across much of the Western U.S.

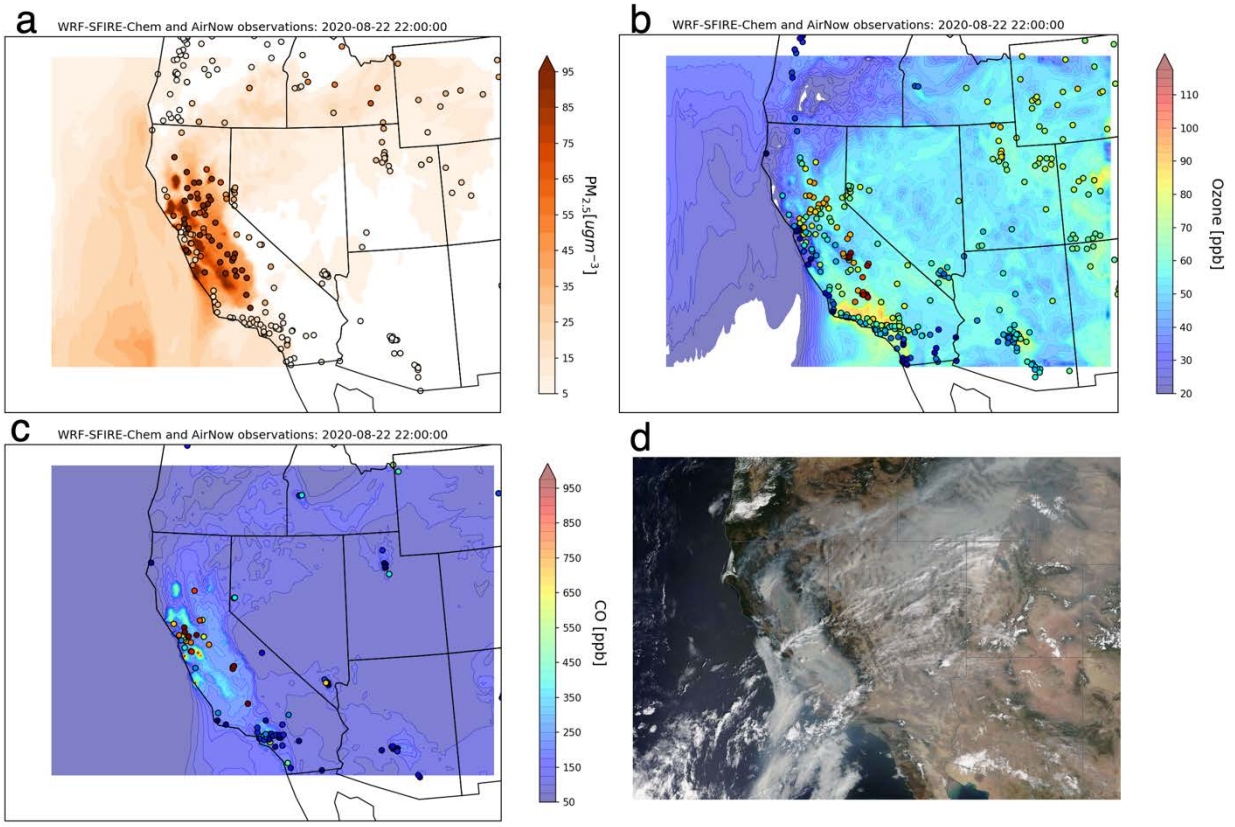

Figure 11. Like Figure 10, but for August 22, 2020.

Overall, WRFSFC generally had a good agreement when modeled concentrations of $PM_{2.5}$, O_3, and CO when compared to air quality observations across the Western U.S. (Figures 10 & 11). On August 21, much of the Central Valley and Bay Area of California was inundated with heavy smoke with $PM_{2.5}$ observations exceeding 100 µg m^{-3} across many locations (Figure 10a). The baseline simulation was able to reproduce the heavier $PM_{2.5}$ concentrations located inland along with the steady decrease in $PM_{2.5}$ towards the shoreline due to onshore sea breezes. The general orientation and the shape of the modeled smoke plume coming out of California aligned with observed concentrations of $PM_{2.5}$ across southeastern Oregon, southern Idaho, and western Wyoming. Like $PM_{2.5}$, O_3 was moderately elevated across these regions with concentrations ranging between 65-80 ppb across northern California, western Nevada, and southern Idaho. Areas of O_3 enhancements were generally collocated with areas of elevated $PM_{2.5}$. While WRFSFC was able to predict areas of elevated concentrations of CO, these enhancements were often underpredicted (Figures 10 and 11c). However, it should be emphasized that CO observations are relatively limited compared to O_3 and $PM_{2.5}$, thus it is difficult to ascertain whether this is a real model bias or simply due to a sampling issue caused by the limited number of CO observations across the West. While the general transport of smoke was well captured by WRFSFC, the model underpredicted the southward transport of smoke along the Wasatch Front when looking at $PM_{2.5}$ measurements on August 21st (Figure 10a). A preliminary meteorological analysis suggested that WRFSFC may have underestimated weak

northerly winds by ~3 ms^{-1} during this time, which were likely necessary for transporting smoke from the Snake River Plain down into Utah.

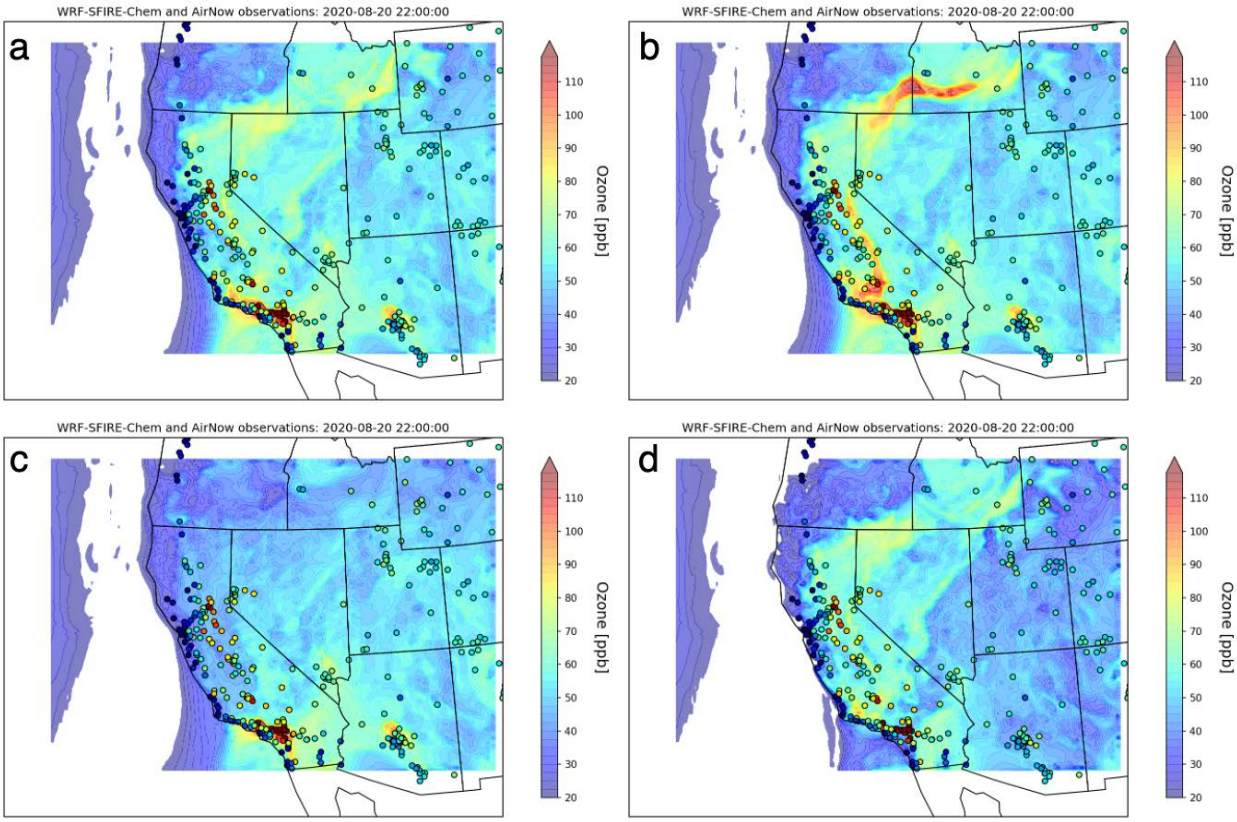

Figure 12. WRFSFC simulated (color-filled contour) and observed O_3 (color-filled circles) concentrations for August 20th, 2020 at 2200 UTC. (a) The baseline WRFSFC simulation, (b) the WRFSFC simulation with aerosol radiative feedbacks turned off, (c) the WRFSFC simulation with fires emissions turned off, and (d) the WRFSFC simulation with anthropogenic emissions turned off.

By August 22nd, $PM_{2.5}$ concentrations across much of the Western U.S. were lower, especially across the Intermountain West (Figure 11). Like the observations, the smoke plume in WRFSFC was much more diffuse relative to August 21st (Figure 10) with $PM_{2.5}$ concentrations ranging from 5-35 μg m^{-3} across the Intermountain West. While the smoke was more diffuse across the Intermountain West, $PM_{2.5}$ concentrations remained highly elevated across the Central Valley of California. O_3 concentrations across the Intermountain West were also lower relative to the previous day.

The next part of our analysis was centered around quantifying the impacts of different emission sources and smoke shading effects on O_3 formation. As described in the **Methods Section**, 4 simulations were generated to analyze O_3 sensitivities across the Intermountain West. The first comparison we look at was O_3 for August 20th during the late afternoon at 2200 UTC, which is when O_3 is usually at its peak concentration. From this analysis, it is evident that wildfires had a substantial impact on O_3 photochemistry across much of the Western U.S. On August 20th, the smoke plume was draped across much of California and up through the Snake River Plain with O_3 (Figure 12) and $PM_{2.5}$ (Figure 13) concentrations being strongly elevated across this region. This is most evident when comparing the baseline WRFSFC run (Figure 12a) with the WRFSFC that turned off fire emissions (Figure 12d). Perhaps unsurprisingly, the average O_3 concentration was highest in the simulation that included all sources of pollutants,

with aerosol radiative feedbacks turned off (Figure 12b). The most optically thick regions of the smoke plume observed O_3 differences that differed by upwards of 30 ppb, indicating that smoke shading had a sizable impact on O_3 production. Areas with the largest decrease in O_3 mostly coincided with regions that had surface-based $PM_{2.5}$ concentrations that exceeded 50-100 μg m^{-3}. This result aligns with the observational-based analysis carried out by Buysse et al. (2019) who found that O_3 production becomes limited when surface-based $PM_{2.5}$ exceed 50 μg m^{-3}.

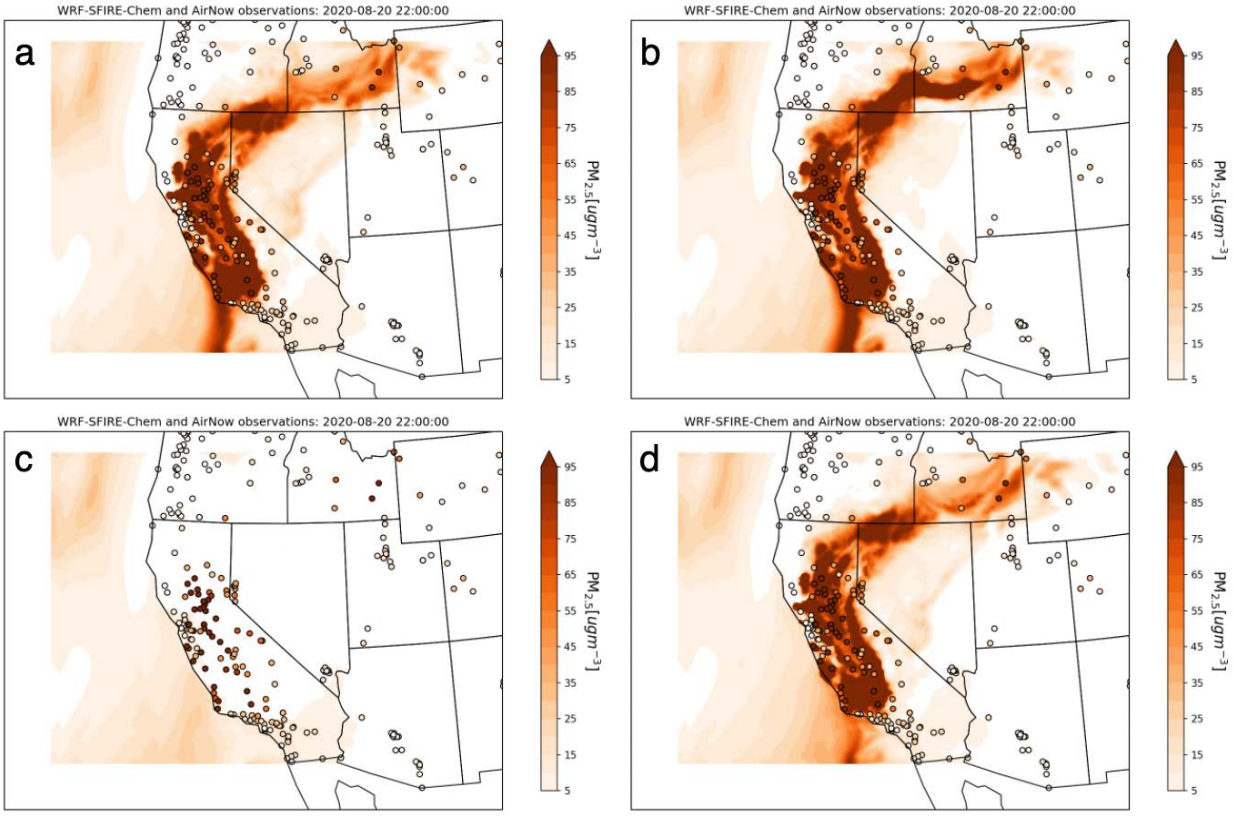

Figure 13. Same as Figure 12 but for $PM_{2.5}$

Another interesting aspect of these results is the impact of smoke shading on smoke transport when comparing the WRFSFC simulations with and without aerosol radiative feedbacks (Figure 13a and Figure 13b). While the smoke plume modeled by both WRFSFC simulations had similar shapes, the location of the highest $PM_{2.5}$ concentrations varied significantly in the downwind section of the plume located over the Intermountain West. For the baseline WRFSFC simulation (Figure 13a), the highest $PM_{2.5}$ concentrations, when excluding California, were located near the Oregon-Nevada border. For the WRFSFC simulation that did not include aerosol radiative feedbacks, the region with the most elevated $PM_{2.5}$ concentrations was more elongated and covered NW Nevada, SE Oregon, and Idaho's Snake River Plain. Here, we suspect that these differences are a consequence of the smoke shading effects impacting regional meteorology. As discussed in Kochanski et al. (2019), smoke shading effects from thick wildfire plumes can alter local meteorology by changing the atmosphere's thermodynamic profile, which results in cooling at the surface and a decoupling of the planetary boundary layer (PBL) from the free troposphere. In turn, this can decrease near-surface winds and limit smoke transport. Previously, this effect was observed only in narrow mountain valleys that were adjacent to large wildfires. The analyses shown here suggest that smoke shading not only affects smoke transport at local scales, but also at the regional scale. Temperature differences

underneath the regional smoke plume in the Snake River Plain were lower by 1-3°C in the simulation that included aerosol radiative feedbacks. PBL heights across this same area were also ~30% lower in the baseline WRFSFC simulation that included aerosol radiative feedbacks. It should be reiterated that fire growth WRFSFC simulations with fire emissions turned on were constrained by a satellite-driven fire growth algorithm and therefore smoke emissions and the fire-generated heat fluxes for each WRFSFC simulation were identical. In summary, shading effects from optically thick smoke plumes not only impact O_3 photochemistry but can also impact how smoke is dispersed downwind of the fire due to changes in meteorology.

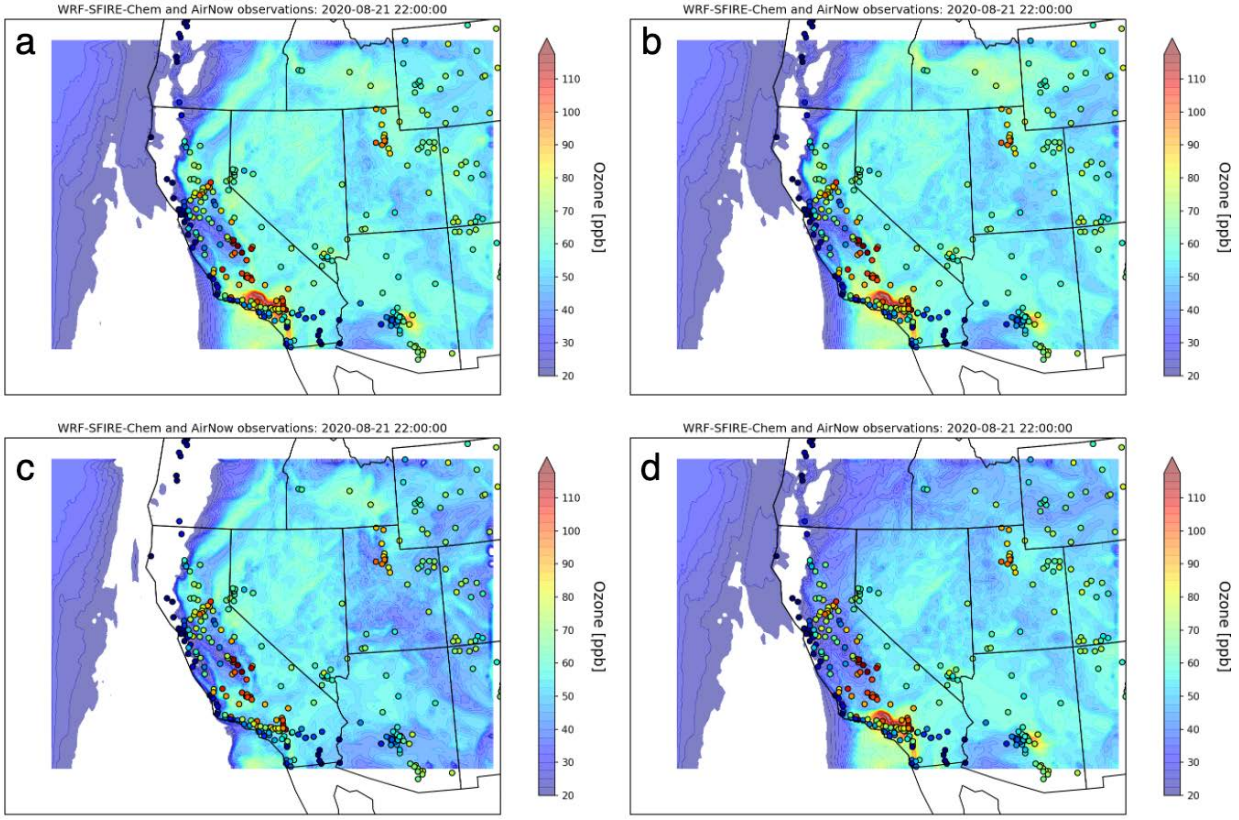

Figure 14. Same as Figure 12, but for August 21, 2020 at 2200 UTC.

While O_3 and smoke impacts were underpredicted across the SLV on August 21, 2020, part of the plume was still advected into the northern part of Utah (Figure 10a). As a result, there was a noticeable difference in O_3 across the Cache Valley and the extreme northern part of the Wasatch Front in August (Figure 14 & 15c). For the baseline WRFSFC simulation, O_3 averaged between 65-73 ppb across this region, while observed O_3 concentrations averaged around ~90 ppb. However, O_3 was ~5-10 ppb lower in the simulation that did not include fire emissions, suggesting that the remote wildfire smoke had an appreciable impact on O_3 production on this day. With that said, it did appear that the baseline WRFSFC simulation was unable to capture the highest O_3 concentrations on August 21st, which is likely related to the model not advecting enough smoke into the Cache Valley as indicated by the discrepancies between modeled and observed $PM_{2.5}$ (Figure 10a). For the SLV, O_3 was generally underpredicted, even during the non-fire days. The baseline WRFSFC simulation generally captured the variability in O_3 between the afternoon and nighttime, however, simulated O_3 concentrations were underpredicted during the afternoon by 5-20 ppb (Figure 15a). Comparisons were made between observed and

WRFSFC simulated NO_2 across the SLV. NO_2 evaluations indicated that afternoon emissions of NO_2 could be overpredicted by the 2017 NEI, especially along the I-15 corridor. This suggests that the SLV might still be in a strong NO_x limited environment and that NO_x might be titrating O_3 too quickly, especially during the afternoon. Underpredicted daytime O_3 concentrations appeared to be most pronounced in the SLV, while this underprediction was less pronounced in smaller cities like Logan (Figure 15b), Ogden (Figure 15c), and Boise (Figure 15d). Based on the WRFSFC sensitivity tests, anthropogenic emissions appeared to be the largest driver in O_3

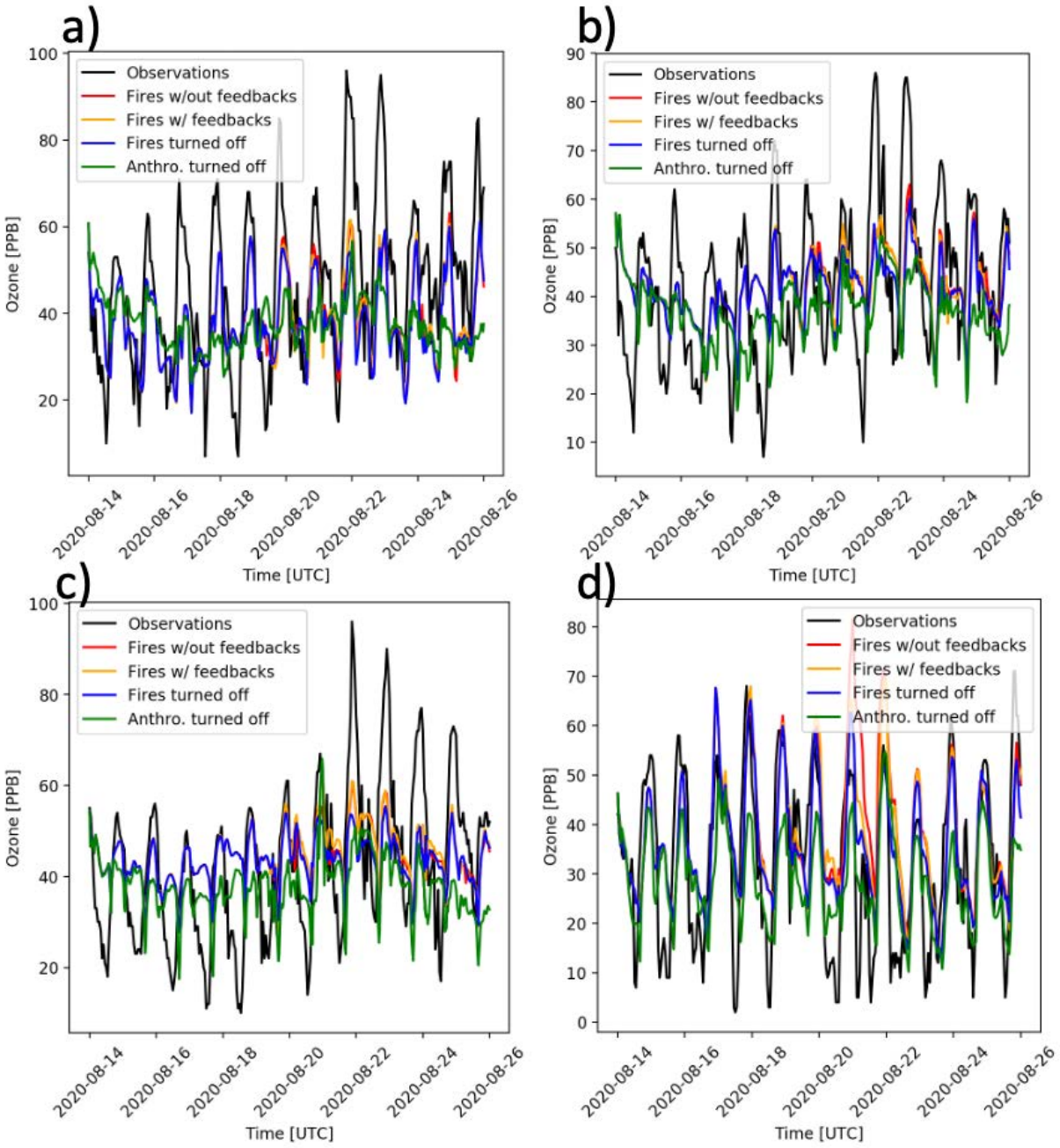

Figure 15. Time series of modeled and observed O3 concentrations at (a) Salt Lake City, (b) Ogden, (c) Logan, and (d) Boise. Observed concentrations are in black, and the WRFSFC simulations for each sensitivity test are colored (red, orange, blue, green).

variability for most days, while wildfire smoke appeared to be of secondary importance in enhancing O_3 concentrations. With that said, smoke was generally underpredicted across most of Utah by WRFSFC, which would have limited modeled O_3 sensitivity to wildfire smoke. Boise, Idaho, which is a mid-sized city in the middle of the wildfire smoke plume, observed large enhancements of O_3 due to wildfire smoke. When smoke emissions were turned off within WRFSFC, O_3 averaged between 55-60 ppb. However, when wildfire smoke emissions were turned on, O_3 was elevated by an additional 10-15 ppb, which is loosely comparable to the difference seen when turning anthropogenic emissions on and off within the WRFSFC (see days before August 20-22 smoke event in Figure 15d). Based on this analysis, we suspect that if WRFSFC meteorology was able to capture the subtle tongue of smoke that drifted down along the Wasatch Front, we would have observed larger O_3 enhancements in the model across northern Utah, like what was observed in Boise.

Future Direction:

Through this project, we developed the very first coupled fire-atmosphere model that can simultaneously resolve smoke plume photochemistry and smoke interactions with other sources of atmospheric pollutants, *e.g., anthropogenic emissions*. This project also led to the development of a new high-density observation network (AirU), which can make measurements of O_3. As part of future work, a study that focuses on synthesizing O_3 measurement from the AirU with high-resolution WRFSFC or WRF-Chem simulations would be valuable for elucidating the processes that govern O_3 production across the SLV.

While simulated atmospheric pollutants within our WRFSFC simulations were in general agreement with regional observations, smoke concentrations during the August 2020 event were largely underestimated along the Wasatch Front. Through our analysis, northern Utah was on the fringes of a regional smoke plume that was primarily centered along the Snake River Plain, where weak northerly winds allowed some smoke to be advected southward along the Wasatch Front. These northerly winds were largely unpredicted by WRFSFC, therefore the model also unpredicted smoke concentrations across Wasatch Front. A much more impactful smoke event was observed on August 6th, 2021, when Utah was in the center of a highly concentrated smoke plume. Many locations across Utah observed $PM_{2.5}$ concentrations that exceeded 200 μg m^{-3}, including the Wasatch Front. Since the smoke transport for the August 2021 case study was driven by a strong storm system, we suspect that WRF might have an easier time simulating this event relative to the August 2020 event (Figure 16). The August 2021 event would also be interesting to investigate since this event was associated with some of the highest $PM_{2.5}$ concentrations ever observed in Utah for a summertime event. Interestingly, the highest $PM_{2.5}$ concentrations observed during this event coincided with relatively low O_3 concentrations (50-60 ppb). This

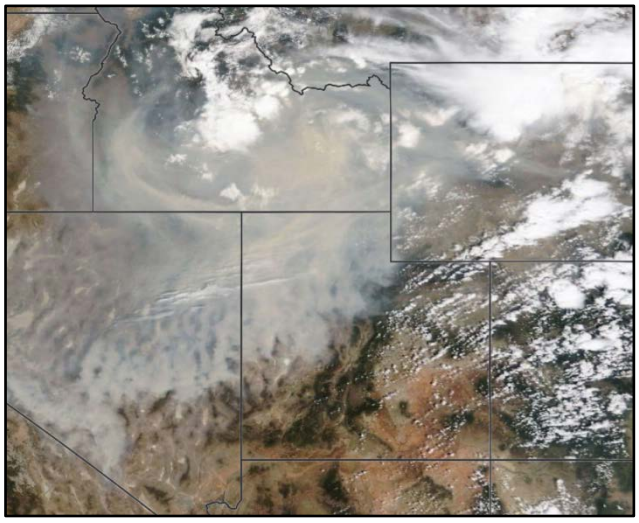

Figure 16. MODIS visible satellite image of the August 6th, 2021 smoke event for Utah.

suggests that heavy smoke may have suppressed O_3 production on this day due to aerosol radiative feedbacks, i.e., smoke shading effects. This case study would likely provide researchers with another opportunity to study how smoke shading impacts surface-based O_3 in urban centers. Such an analysis would be insightful in the context of O_3 forecasting.

For this project, we utilized the 2017 NEI to develop our anthropogenic emissions inventory. For future work, we would propose using a new higher resolution emission inventory product that is currently being developed by National Oceanic and Atmospheric Administration (NOAA) Chemical Sciences Laboratory. This emission product has a detailed vehicle emissions model, which may provide better estimates for traffic emissions and may help improve O_3 simulations across the SLV.

Data and Code Management:

The WRFSFC model simulations generated for this analysis are hosted by the University of Utah's Center for High Performance Computing. The WRFSFC simulations can be downloaded from a public-facing website, also hosted by CHPC: https://home.chpc.utah.edu/~u0703457/UDAQ_2020-2022/

WRFSFC output files are in a Network Common Data Form file format, and include gridded concentrations of atmospheric pollutants, along with meteorology. The files also contain information for geolocating the location of each grid cell. Each directory in the link provided above corresponds to the different WRFSFC sensitivity tests carried out as part of this experiment. For example, the baseline simulation, which includes all potential emission sources, along with aerosol radiative feedbacks can be found in the directory called '*WRFSFC_fire_on_aer_on*'. The simulation with all emission sources, with radiative feedbacks turned off can be found in the directory named '*WRFSFC_fire_on_aer_off*'. The simulation where fire emissions were turned off can be found in 'WRFSFC_no_fire'. Lastly, two simulations were generated where anthropogenic emissions were turned off, and aerosol radiative feedbacks turned on (*WRFSFC_no_anthro_aer_on*) and off (*WRFSFC_no_anthro_aer_off*). Each of these directories contains the namelist files used to create these simulations. Air quality observations downloaded from the AirNow data repository, and the scripts used to generate the analysis shown here can be found in the folder named "*obs_and_scripts*". The postprocessing code used for our analyses was written in python and is in a Jupyter notebook format.

The WRFSFC runtime code is publicly on Github: https://github.com/openwfm/WRF-SFIRE. Code related to chemical emission and boundary condition processing outlined in the methodology section is publicly available at NCAR: https://www2.acom.ucar.edu/wrf-chem/wrf-chem-tools-community

Acknowledgments:

Computing resources at the University of Utah's Center of High Performance Computing (CHPC) and the NCAR-Wyoming Supercomputing Center were used to carry out our modeling analyses. We would like to thank the Utah Transit Authority for supporting the installation and maintenance of the instrumentation on TRAX, which was used to evaluate the Ozone low-cost sensor data. Lastly, we would like to thank Dr. William Lassman at Lawrence Livermore National Laboratory for providing guidance on processing the chemical data for WRFSFC.

Bibliography:

Buysse, C. E., A. Kaulfus, U. Nair, and D. Jaffe (2019), Relationships between Particulate Matter, Ozone, and Nitrogen Oxides during Urban Smoke Events in the Western US. *Environ. Sci. Technol.*, 53(21), 12519–12528.

Buchholz, R. R., L. K. Emmons, and S. Tilmes (2019), CESM2.1/CAM-chem Instantaneous Output for Boundary Conditions. UCAR/NCAR - Atmospheric Chemistry Observations and Modeling Laboratory. https://doi.org/10.5065/NMP7-EP60.

Emmons, L. K., et al. (2010), Description and evaluation of the Model for Ozone and Related chemical Tracers, version 4 (MOZART-4). *Geosci. Model Dev.*, 3, 43–67.

Farguell, A., J. Mandel, J. Haley, D. V. Mallia, A. K. Kochanski, and K. Hilburn (2021), Machine learning estimation of fire arrival time from level-2 active fire satellite data. *Remote Sensing*, 13(11), 2203.

Grell G. A., S. E. Peckham, S. McKeen, R. Schmitz, G. Frost, W. C. Skamarock, and B. Eder (2005), Fully coupled 'online' chemistry within the WRF model. *Atmos. Environ*., 39, 6957–6975.

Guido, A. and S. Muller (2016), Introduction to Machine Learning with Python. Available online at: https://python-course.eu/machine-learning/.

Jaffe, D. and J. Ray (2007), Increase in surface ozone at rural sites in the western US. *Atmos. Environ.*, 41, 5452–5463.

Kochanski, A. K., M. A. Jenkins, K. Yedinak, J. Mandel, J. Beezley, and B. Lamb (2016), Toward an integrated system for fire, smoke, and air quality simulations. *Int. J. Wildland Fire,* 25, 558–568.

Kochanski, A. K., D. V. Mallia, M. Fearon, T. Brown, and J. Mandel (2019), Modeling wildfire smoke feedback mechanisms using a coupled fire-atmosphere model with a radiatively active aerosol scheme. *J. Geophys. Res.*, 124(16), 9099–9116.

Kochanski, A. K., F. Herron-Thorpe, D. V. Mallia, J. Mandel and J. K. Vaughan (2021), Integration of a coupled fire-atmosphere model into a regional air quality forecasting system for wildfire events. *Front. For. Glob. Change*, 4:728726.

Liu J. C., L. J. Mickley, M. P. Sulprizio, F. Dominici, X. Yue, K. Ebisu, G. B. Anderson, R. F. A. Kahn, M. Bravo, and M. I. Bell (2016), Particulate air pollution from wildfires in the Western US under climate change. *Clim. Change*, 138 655–666.

Mallia, D. V., A. Kochanski, K. E. Kelly, R. Whitaker, W. Xing, L. Mitchell, A. Jacques, A. Farguell, J. Mandel, P.-E. Gaillardon, T. Becnel, and S. Krueger (2020), Evaluating wildfire smoke transport within a coupled fire-atmosphere model using a high-density observation network for an episodic smoke event along Utah's Wasatch Front. *J. Geophys. Res.*, 125, e2020JD032712.

Mandel, J., J. D. Beezley, A. K. Kochanski (2011), Coupled atmosphere-wildland fire modeling with WRF 3.3 and SFIRE 2011. *Geosci. Model Devel.,* 4, 591–610.

McClure, C. D., and D. A. Jaffe (2018), US particulate matter air quality improves except in wildfire-prone areas. *Proc. Natl. Acad. Sci.*, 201804353.

Mitchell, L. E., E. T. Crossman, A. A. Jacques, B. Fasoli, L. Leclair-Marzolf, J. Horel, D. R. Bowling, J. R. Ehleringer, and J. C. Lin (2018), Monitoring of greenhouse gases and pollutants across an urban area using a light-rail public transit platform. *Atmos. Environ.*, 187, 9–23.

Ninneman, M., and D. A. Jaffe (2021), The impact of wildfire smoke on ozone production in an

urban area: Insights from field observations and photochemical box modeling. *Atmos. Environ.*, 267,118764.

Okorn, K., and M. Hannigan (2021), Improving air pollutant metal oxide sensor quantification practices through: An exploration of sensor signal normalization, multi-sensor and universal calibration model generation, and physical factors such as co-location duration and sensor age. *Atmosphere*, 12, 645.

Spracklen, D. V., L. J. Mickley, J. A. Logan, R. C. Hudman, R. Yevich, M. D. Flannigan, and A. L. Westerling (2009), Impacts of climate change from 2000 to 2050 on wildfire activity and carbonaceous aerosol concentrations in the western United States. *J. Geophys. Res.*, 114, D20301.

Saha, S., et al. (2014), The NCEP climate forecast system version 2. *J. Climate*, 27(6), 2185–2208.

Sayahi, T., A. Garff, T. Quah, K. Lê, T. Becnel, K. M. Powell, P.-E, Gaillardon, A. E. Butterfield, and K. E. Kelly (2020), Long-term calibration models to estimate ozone concentrations with a metal oxide sensor, *Environ. Pollut.*, 267, 115363.

Verma, S., and Coauthors (2009), Ozone production in boreal fire smoke plumes using observations from the Tropospheric Emission Spectrometer and the Ozone Monitoring Instrument. *J. Geophys. Res.*, 114, D02303.

Westerling, A. L., H. G. Hidalgo, D. R. Cayan, and T. W. Swetnam (2006), Warming and earlier spring increases western U.S. forest fire activity. *Science*, 313, 940–943.

Wilmot, T. Y., A. G. Haller, J. C. Lin, and D. V. Mallia (2021), Expanding number of Western US urban centers face declining summertime air quality due to enhanced wildland fire activity. *Environ. Res. Lett.*, 16, 054036.

Yokelson, R. J., and Coauthors (2011), Coupling field and laboratory measurements to estimate the emission factors to identified and unidentified trace gases for prescribed fires. *Atmos. Chem. Phys.*, 13, 89–116.